Available online at www.sciencedirect.com
ScienceDirect
Journal of Nuclear Materials 361 (2007) 262–273
journal of nuclear materials
www.elsevier.com/locate/jnucmat

Synergistic effects of interstitial impurities and radiation defects on mechanical characteristics of ferritic steels

I. Charit [a], C.S. Seok [b], K.L. Murty [a,*]

[a] North Carolina State University, Raleigh, NC 27695-7909, USA
[b] Sungkyunkwan University, Suwon, Republic of Korea

Abstract

Ferritic steels are generally used in pressure vessels and various reactor support structures in light water reactors. They are known to exhibit radiation embrittlement in terms of decreased toughness and increased ductile–brittle transition temperature as a result of exposure to neutron radiation. The superimposed effects of strain aging due to interstitial impurity atoms on radiation embrittlement were considered first by Wechsler, Hall and others. Here we summarize some of our efforts on the investigation of synergistic effects between interstitial impurity atoms (IIAs) and radiation-induced point defects, which result in interesting effects at appropriate temperature and strain rate conditions. Two materials, a mild steel and a pressure vessel steel (A516 Gr.70), are evaluated using tensile and three-point bend tests.

1. Introduction

Ferritic steels are used as pressure vessel materials, various reactor support structures in light water reactors, and steam generator housings in liquid metal fast breeder reactors. For a long time, it has been known that radiation embrittlement is a major concern for ferritic steels in pressure boundary applications [1]. However, an attractive combination of properties with favorable pricing of ferritic steels has encouraged researchers to understand and minimize/eliminate these problems. A clear manifestation of radiation embrittlement of the ferritic steels is an increased ductile–brittle transition temperature (DBTT) along with decreased energy to fracture. It was also shown that regions like heat-affected zones in the welded steel parts under radiation exposure are more susceptible to radiation embrittlement. Reactor Vessel Surveillance Programs (RVSP) in operating nuclear reactors revealed that the radiation embrittlement of these steels are generally influenced by three major factors, fast neutron fluence, irradiation temperature and chemical compositions [1]. Effects of copper, nickel, phosphorus etc., present as alloying or impurity elements have been found to be particularly detrimental in aggravating radiation embrittlement phenomena. Fig. 1(a) and (b) demonstrates how the increasing copper content increases the DBTT

* Corresponding author. Tel.: +1 919 515 3657; fax: +1 919 515 5115.
E-mail addresses: icharit@ncsu.edu (I. Charit), csseok@yurim.skku.ac.kr (C.S. Seok), murty@ncsu.edu (K.L. Murty).

0022-3115/$ - see front matter © 2006 Elsevier B.V. All rights reserved.
doi:10.1016/j.jnucmat.2006.12.003

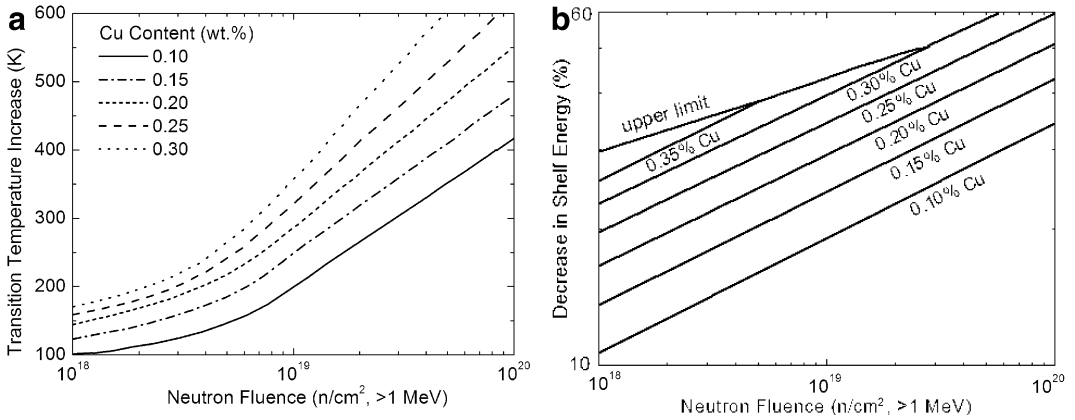

Fig. 1. Curves predicting (a) increase in DBTT and (b) decrease in shelf energy as a function of neutron fluences for various copper concentrations (in wt%).

(which may be as high as a few hundred K) and lowers the upper shelf energy as a function of fast neutron fluence [2]. Atom Probe Field Ion Microscopy (APFIM) and Small Angle Neutron Scattering (SANS) revealed that Cu-vacancy clusters produced during irradiation might be responsible for these effects while Positron Annihilation Spectroscopy (PAS) measurements pointed out that radiation-induced precipitation of carbides and nitrides might be the prime reason behind the embrittlement of RPV steels [3,4]. Although these observations have been found to be true in numerous cases, the underlying physical mechanisms are not clearly established. It is instructive to note that significant work is being done to understand the interaction characteristics between alloying elements and radiation produced defects, and their influence on mechanical properties using multiscale modeling approaches [5].

The role of IIAs in radiation embrittlement is not clearly established. However, strain aging effects whereby dislocations get locked by the IIAs lead to reduced ductility and fracture toughness even without irradiation while these IIAs interact with point defects produced during irradiation that might further lead to reduction in fracture toughness. Studies on both static and dynamic strain aging of irradiated steels have revealed that the concentration of IIAs in solution decreases with radiation, thereby increasing the temperature range at which the aging phenomena occur [2,4].

Dynamic strain aging (DSA) refers to a discontinuous plastic flow that takes place as a result of periodic locking and unlocking of mobile dislocations by solute atmospheres; the phenomenon is also known as Portevin–Le Chatelier (PLC) effect [6]. This is also manifested by short periodic serrations in the stress–strain curves. DSA has traditionally been observed during deformation of dilute alloys at moderate temperatures and certain strain rate regimes [6]. DSA is largely considered an unwanted phenomenon because it results in a loss of ductility and negative strain rate sensitivity, thus adversely affecting mechanical and fracture properties. This phenomenon in steels is generally termed as blue-brittleness since they occur typically above 373 K depending upon steel composition. The serrated flow characteristics of low-carbon steels in the blue-brittle regime were discussed by Hall [6]. Although several models have been proposed to elucidate DSA, there is still a lack of universal models capable of explaining the behavior in different alloys [7]. The goal of the present paper is to illustrate the superimposed effects of DSA and radiation-produced defects on the mechanical properties of various iron-based alloys. It has been shown earlier that the presence of the radiation effects may suppress the DSA effect, and rather improves the ductility and fracture characteristics of the irradiated mild steels under appropriate temperatures and strain rate ranges [2,4] albeit the temperature range of DSA increases with increased dose. The kinetics of aging can be well studied by examining the strain rate and temperature effects of DSA as well as static strain aging at varied temperatures. Similarities between radiation exposure and denitriding clearly indicate the fact that neutron irradiation results in reduced IIAs in solution.

Radiation hardening can be described by partitioning the yield stress into two components namely

friction and source hardening terms similar to the Hall–Petch relation [8]:

$$\sigma_y = \sigma_i + \sigma_s = \sigma_i + \frac{k_y}{\sqrt{d}}, \quad (1)$$

where k_y is the Hall–Petch coefficient, and d is the grain size. The stress required for unlocking the pinned dislocations and set them free into motion is called source hardening (σ_s) whereas the stress experienced by the unlocked dislocations during their movement through the lattice is called friction hardening (σ_i). Friction stress varies directly with the square-root of defect density and thus increases with the square-root of neutron fluence. On the contrary, it has been shown that the source hardening decreases with radiation exposure [9] apparently due to the reduced IIAs in solution. A major implication of yield strength partitioning into two components is that the ductile–brittle transition temperature (DBTT) can be correlated with them using Cottrell's brittle fracture theory [10].

2. Experimental procedures

Two ferrous materials, a silicon-killed mild steel and an RPV ferritic steel (A516) have been considered in this investigation. Their compositions are given in Table 1.

Mild steel wires of 0.001 m diameter and 0.0385 m gage length were used. The main advantage of wire tensile specimen is that a Luders band is nucleated near one grip and propagates to the other end in a stable fashion so that the lower yield stress remains extremely constant. The material was cold drawn from a rimmed mild steel, and the prepared specimens were annealed under vacuum at various combinations of temperature and time to get a grain diameter between ASTM grain size 5 (62 μm) and 8 (22 μm).

Denitriding of mild steel was carried out in a furnace under a dry hydrogen atmosphere. Different levels of nitrogen were obtained by annealing at 948 K for various times followed by vacuum annealing at 773 K for the dual purpose of homogenization and to maintain approximately constant grain size.

Vacuum-annealed samples were irradiated in the heavy-water moderated, high-isotope-flux Australian reactor (HIFAR) at Lucas Heights. Different neutron doses were obtained by inserting the samples in vertical holes, at positions close to the fuel plates for high doses, and at positions away from the plates for low doses. However, the irradiation time was kept the same. The actual neutron fluxes were calculated from the γ-activity of ^{46}Ti wire monitors placed near the specimen cans, and thus four fluence levels (>1 MeV) were obtained. Special precautions were taken to reduce the γ-heating of the specimens, and the irradiation temperature was taken as ~353 K, the heavy-water temperature. The irradiated specimens all became very radioactive because of the high neutron capture cross-section of ^{58}Fe. They were kept in a lead coffin until they become cold (i.e. free of any radioactivity). All tensile tests were performed on a hard tensile machine of the type designed by Adams [11]. The cross-head speed was varied between 1.8×10^{-7} and 1.0×10^{-7} m s^{-1}.

Forged plates of A516 Gr.70 steel were received in two lots. Subsize tensile and V-notched three-point bend specimens were machined. Samples of A516 Gr.70 steel were sealed in evacuated quartz tubes, and irradiated in the PULSTAR reactor at the North Carolina State University. Much details of the experimental procedure have been described elsewhere [12].

3. Results and discussion

3.1. Mild steel

3.1.1. Effect of fluence on yield stress

It is well known that the neutron exposure hardens materials. Tensile stress–elongation curves of mild steel (38 μm grain size) at 300 K, irradiated at various neutron fluences, are shown in Fig. 2. It has been noted that the highest neutron fluence of 1.4×10^{19} n/cm^2 leads to an almost rounded shape

Table 1
Chemical compositions of the materials studied (in wt%)

Material	C	Mn	Si	S	P	Cu	Mo	Cr	Ni
Mild steel	0.05	0.39	0.001	0.012	–	0.091	–	0.0041	0.032
A516Gr.70	0.20	0.98	0.02	0.02	0.02	0.24	0.03	0.20	0.16

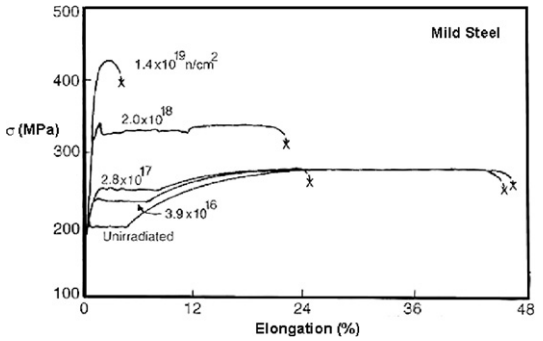

Fig. 2. The effect of neutron fluence on the tensile response of mild steel at 300 K.

of yield region. An increase in the lower yield stress upon neutron exposure is given by [12,13]

$$\Delta\sigma_{LY} = \sigma^{i}_{LY} - \sigma^{o}_{LY} = B(\phi t)^{1/3}, \quad (2)$$

where σ^{i}_{LY} and σ^{o}_{LY} are the lower yield stresses at ambient temperature for irradiated and unirradiated materials, respectively, and ϕ is the neutron flux and t is the irradiation time (ϕt is the fluence). The constant 'B' value is about 91.7 if the stress values are in Pa and fluence in n/cm^2. 'B' values were found to be 99.6 and 81.4 for mild steels with grain sizes of 27 and 53 μm, respectively [13]. Cottrell [14] obtained a 'B' value of 55.16 for an En2 mild steel irradiated at 373 K in the BEPO reactor. This value is close to what was obtained for the mild steels, however, the difference may have come from the variation in composition and reactor features. Hence, the value of 'B' has been found to decrease slightly with increasing grain size, implying that the fine grained material may be less resistant to radiation hardening. Similar conclusions were drawn by Castagna et al. [15] for Fe–Ti alloys, and by Trudeau [16] in Ni-bearing steels. However, it should be noted that this observation is in contradiction with Cottrell's prediction that fine grained steels will have superior resistance to radiation hardening [17]. Similar measurements on a decarburized mild steel with a grain size of 44 μm yielded an 'B' value of 126.5, implying that the interstitial-free steel will be less resistant to radiation hardening. A cube-root dependence is observed experimentally, whereas a square-root dependence is expected if one assumes that the irradiation does not affect the unpinning constant, k_y in the Hall–Petch relation (Eq. (1)).

Luders elongation (ε_{LB}) was also found to vary with fluence in a similar manner as the lower yield

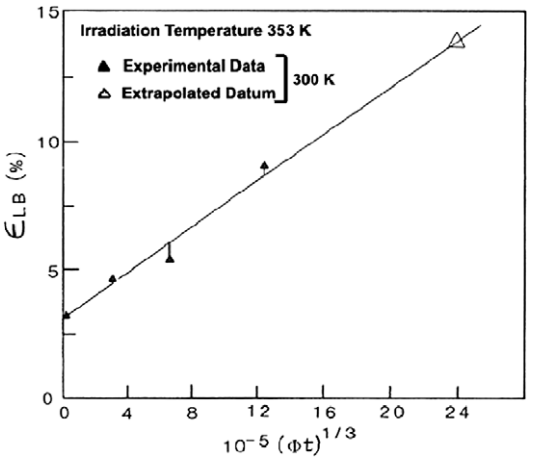

Fig. 3. Luders strain as a function of fluence in the irradiated mild steel.

stress as discussed in the previous paragraph. Fig. 3 illustrates the linear relationship between Luders strain and the cube-root of fluence. This is expected since it is known that the Luders strain is proportional to the yield strength in steels. An extrapolation to a neutron fluence of 1.4×10^{19} n/cm^2 shows that the Luders elongation would reach ~13%. However, in reality fracture occurred before reaching this elongation (Fig. 2).

Using the extrapolation technique proposed by Makin and Minter [18], the source hardening and friction hardening components are evaluated. The friction hardening component indeed increased with a square-root dependence of fluence (Fig. 4). Thus, it is in line with our understanding of friction hardening that the dislocations motion is hindered by the effect of mobile dislocations, producing long-range interactions with forest dislocations and short-range

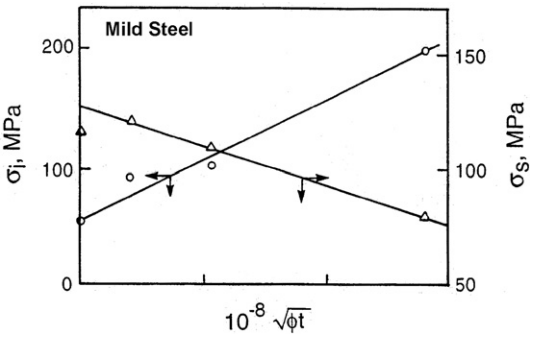

Fig. 4. Calculated source and friction hardening components of yield stress as a function of neutron fluence in mild steel (38 μm grain size) [12].

interactions with radiation-produced defects [13]. Considering that the defect density increases linearly with fluence, one obtains a square-root dependence. However, it is also noted that the source hardening decreases with neutron fluence as shown in Fig. 4. This is the reason why the yield stress shows a slightly decreased influence of neutron fluence (cube-root versus square-root). Thus neutron radiation exposure results in decreased Hall–Petch constant (k_y). A good correlation is noted between the results obtained from extrapolation technique and from Eq. (1) using mild steels of various grain sizes [12]. In Armco iron with 50 μm grain size, the unpinning constant value changed from 390 to 300 MPa $\mu m^{1/2}$ under a neutron fluence value of 5×10^{17} n/cm^2 (>1 MeV) [12].

3.1.2. Role of interstitial elements in steels

The yield point phenomenon observed in ferritic low-carbon steels occurs because of dislocation locking by carbon and nitrogen interstitial atoms, as also serrated flow effects or PLC effect. However, strain aging effects in slowly cooled samples are primarily due to nitrogen since most of the carbon atoms precipitate out of solution forming iron-carbide (i.e. cementite) leaving very small concentration of carbon atoms in solution at room temperature. Conversely, a higher amount of nitrogen atoms (in some cases, about 10 times) up to about 250 °C remain as interstitial solutes in solution as compared to carbon atoms, and thus, instrumental in producing aging effects [19]. The experimental conditions (temperatures and strain rates) at which serrated flow is observed are critically influenced by the available interstitial impurities in solution, specifically nitrogen. Nitrogen exerts more influence on DSA because of their higher solubility and mobility when compared to those of carbon atoms.

There may be two main mechanisms by which nitrogen in solid solution affects the radiation damage process in steels [20]. First, self-interstitial atoms move towards the nitrogen atoms and thus are not available for hindering the dislocation motion [21]. Second, nitrogen atoms move towards the radiation-produced defect clusters during irradiation and get trapped in the small vacancy loops or interstitial-type faulted dislocation loops lying on {1 1 0} planes. This process is expected to result in more hardening since the presence of nitrogen atoms residing inside the faulted loop resists the unfaulting of the loop into becoming glissile perfect loops by shearing. At low nitrogen concentrations, the first process is believed to operate. Little and Harries [22] observed that there is a threshold amount of nitrogen concentration above which the second process dominates. However, this threshold amount may depend upon many factors such as the specific alloy composition, neutron energy spectrum, irradiation temperature and so forth.

In Fig. 5, a series of stress–elongation curves for a vacuum-annealed mild steel are shown as a function of tensile test temperature. At room temperature, the stress–elongation curve is smooth. At 363 K, there appear random load drops (referred to as jerky flow) in the flow curve region, but the Luders plateau remains largely smooth. At the lower critical temperature (413 K), random stress 'pips' are observed in the Luders plateau, while more periodic stress drops (known as serrated flow) are identified in the flow curve. At still higher temperatures, the serrations in the Luders band regime become higher accompanied by serrations in the flow curve. At about 489 K, the flow curve becomes largely smooth with occasional bands of serrations whereas the serrations still appear in the Luders regime. Finally at 544 K and above, all serrations disappeared with essentially no Luders elongation.

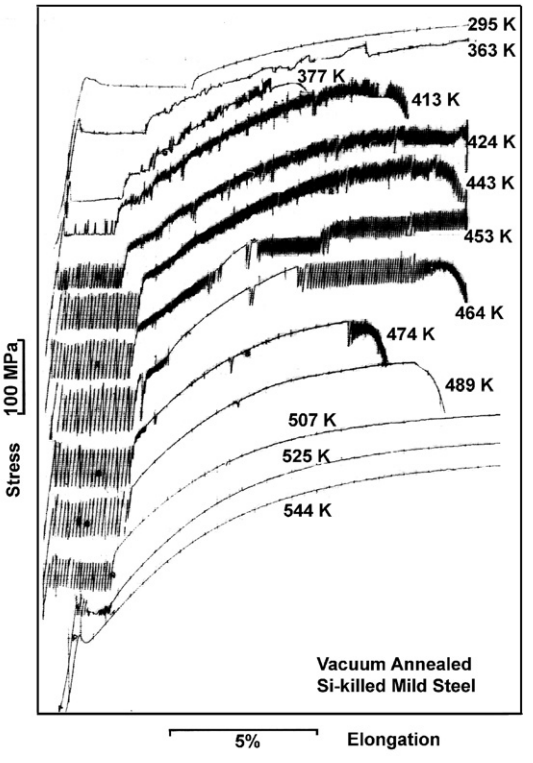

Fig. 5. Stress–elongation curves at different temperatures.

Investigating the strain rate dependence of the lower critical temperature yielded an activation energy value of $\sim$75 kJmol^{-1}, which is close to that of carbon and nitrogen diffusion in alpha-iron [23].

Effects of test temperature on yield stress, tensile strength (UTS) and total elongation to fracture are shown in Fig. 6, where we note an athermal region in the yield stress in DSA regime. This reflected as a peak in UTS while as a dip in ductility. It is interesting to note that distinct dips in elongation appear at the lower critical temperature with the onset of serrated yielding and at the higher critical temperature corresponding to the disappearance of serrations.

As discussed earlier, neutron radiation exposure produces both point and line defects. Early work by Murty and Hall [23] revealed that the interstitial impurity atoms (IIAs) combine with these radiation-produced defects, leading to the formation of defect complexes resulting in decreased net concentration of IIAs in solution. Fig. 7 shows stress–strain curves for the irradiated mild steel (neutron fluence 3.9×10^{16} n/cm^2).

Further, the stress–strain curves for samples irradiated at other neutron fluences are also examined. Two clear observations from these data are: (a) the critical temperature for the onset of DSA was increased, and (b) the temperature range of DSA was narrowed. In addition, the height of serrations in the Luders regime decreased. With increasing neutron fluence, the serration height progressively decreased. At neutron fluence at or greater than 10^{17} n/cm^2, the load drops become random and small (characteristic of jerky flow). At the highest fluence (1.4×10^{19} n/cm^2), pronounced radiation embrittlement is observed with no evidence of serrated flow.

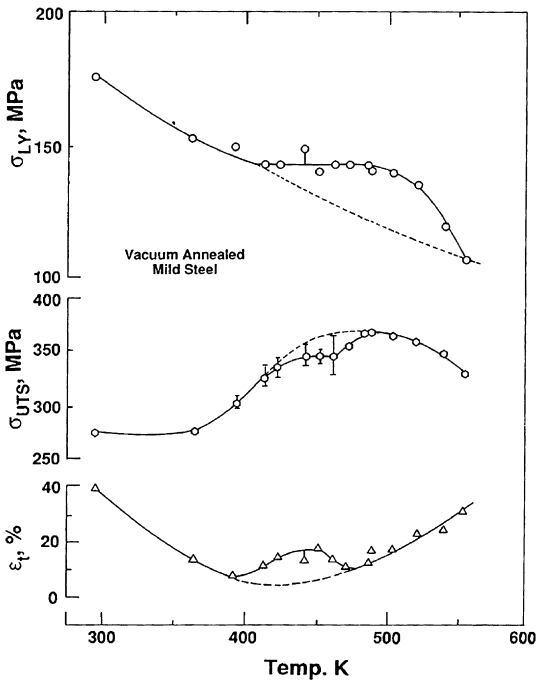

Fig. 6. Temperature dependence of yield stress, ultimate tensile strength and total elongation.

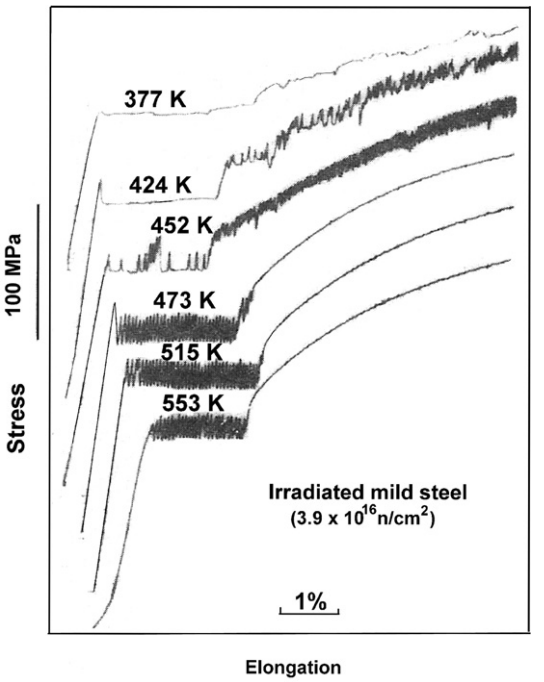

Fig. 7. Stress–strain curves for the irradiated mild steel.

Murty and Mahmood [24] treated the mild steel in dry hydrogen atmosphere for various times. The corresponding stress–strain curves for these samples are quite similar to those of the neutron irradiated mild steel (Fig. 8) with an upward shift of the lower temperature at which DSA appears and the noticeable decrease in the height of serrations. Fig. 8 depicts the stress–strain curves for a sample dry hydrogen treated for 1.04×10^4 s (with a residual nitrogen content of 0.002 at.%). It is found that the reduction in nitrogen content increases the lower critical temperature, decreases the maximum height of serrations, and decreases the upper critical temperature. Fig. 9 shows the effect of strain rate on the serration height as a function of temperature. Increasing strain rate results in increased lower critical temperature increases more than in the increase of upper critical

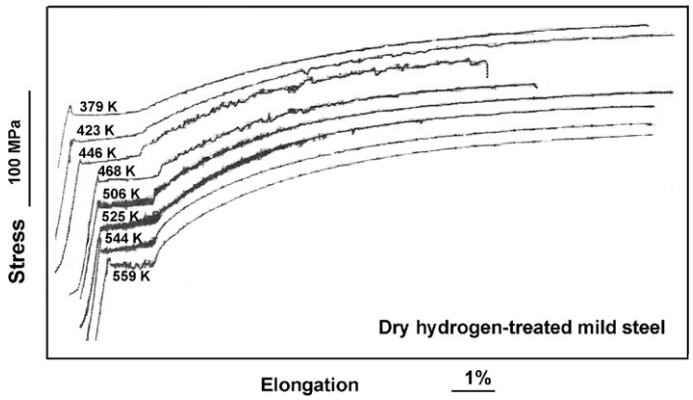

Fig. 8. Stress–elongation curves for partially denitrided mild steels, at varied test temperatures.

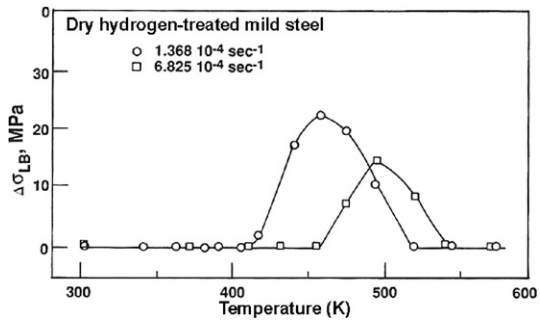

Fig. 9. Effect of strain rate on temperature variations of serration height in Luders elongation for partially denitrided steel ($c = 0.0096$ a/o N).

temperature leading to decreased DSA region. Also, the serration heights decreased with increasing strain rate. At further higher strain rates, it is expected that serrations may not appear at all.

It is clear that increasing the radiation dose and decreasing the nitrogen concentration have strikingly similar effect on the stress–strain curves of the mild steel. Thus, it supports the postulate that the content of IIAs in solution decreases following radiation exposure. Further, Murty [13,23] studied the effect of neutron radiation dose on static strain aging kinetics. It was demonstrated that at high radiation fluence, the steel becomes non-aging. Again, the results corroborate the fact that IIAs combine with the radiation-produced defects, which is rather responsible for increase in friction hardening. On the other hand, there is less amount of free IIAs present in solution and they can not form solute atmospheres to effectively lock the dislocations in order to manifest the DSA effects. McLennan and Hall [25] and Wagenblast and Damask [26] demonstrated through internal friction experiments that the concentration of carbon atoms is significantly reduced from solid solution in irradiated Fe–C alloys. Wechsler and Murty [4] reviewed the possible mechanism of combination of radiation-produced defects and IIAs.

Fig. 10 is an Arrhenius plot of the strain rate and lower critical temperatures for vacuum-annealed, partially denitrided (0.002 at.% N) and irradiated mild steels. Parallel lines were obtained for all the materials, yielding essentially the similar activation energy ($\sim$75 kJmol^{-1}). As noted in earlier section, this value is close to the activation energy for the

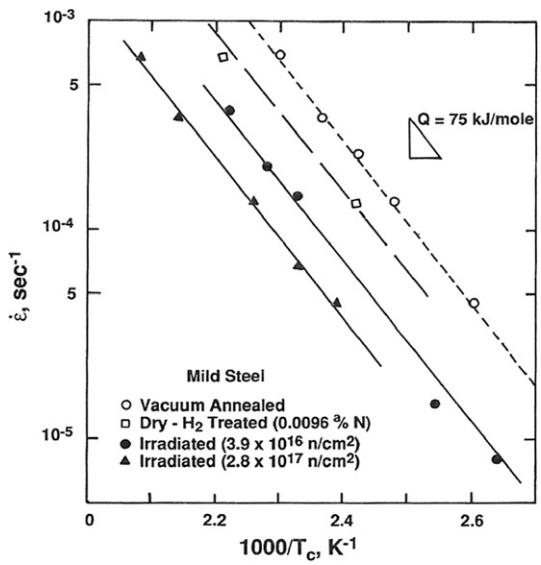

Fig. 10. Arrhenius plot of the strain rate versus lower critical temperature for vacuum-annealed, partially denitrided and irradiated mild steel.

migration of carbon/nitrogen in alpha-iron. It is interesting to note that a reduction in nitrogen content or exposure to neutron irradiation does not change the kinetics of the serrated flow.

3.1.3. Interaction between IIAs and radiation-produced defects – synergistic effect

It has been amply demonstrated in the previous sections that reduced net concentration of IIAs in solution following exposure to neutron radiation reduces the effect of DSA or 'blue-brittleness' even though the radiation hardening still accompanies. Naturally, the natural curiosity would be to ascertain the fate of ductility under neutron radiation exposure with suppression of DSA. Fig. 11 includes the tensile stress–strain curves at 373 K showing the effect of neutron radiation exposure. It clearly shows that there is an intermediate neutron dose at which DSA effect is suppressed and there is a concomitant increase in ductility. For instance, there is a 84% increase in the lower yield stress accompanied by 177% increase in ductility at 373 K, following exposure to a neutron fluence of 2×10^{18} n/cm^2 [27]. Fig. 12 shows the variation of elongation (top) and yield stress (bottom) as a function of test temperature. We note that the ductility increases in a certain temperature regime following exposure to neutron radiation. This regime is where DSA predominated in the unirradiated sample. Similarly, the energy to fracture in the irradiated mild steel was found to vary in a similar fashion.

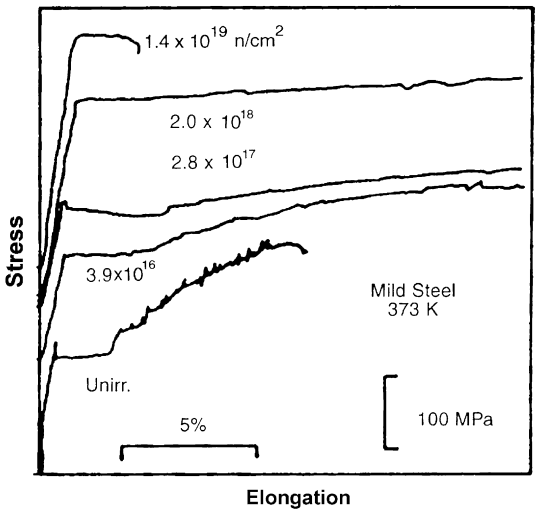

Fig. 11. Effect of neutron irradiation on tensile stress–strain curves for mild steel at 373 K.

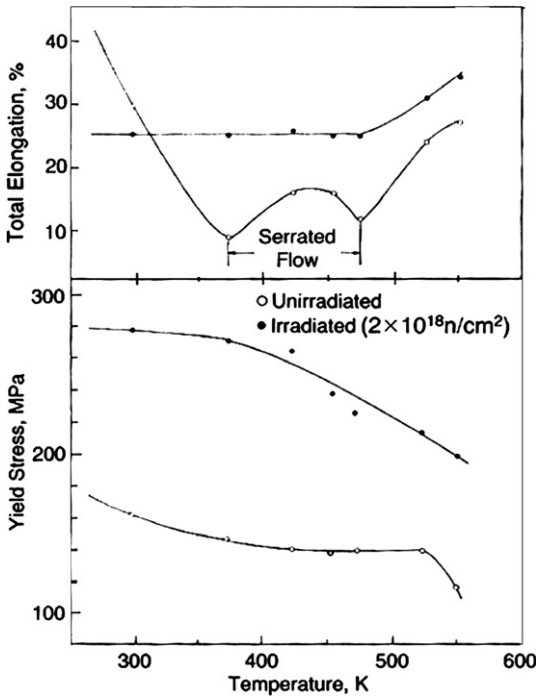

Fig. 12. The variation of ductility and yield stress as a function of testing temperatures.

3.1.4. Theoretical treatment

Van de Beukel and Kocks [28] developed a model that relates the impurity concentration (c) and its diffusivity (D) for deformation under a given strain rate to attain a similar degree of locking. Accordingly,

$$c = KD^{-2/3}. \tag{3}$$

The activation energy for locking is then given by

$$Q = \frac{3}{2}\frac{\mathrm{d}\ln c}{\mathrm{d}(1/kT)}. \tag{4}$$

Fig. 13 is an Arrhenius plot of the nitrogen concentration versus the lower critical temperature and the line drawn through the data points yields an activation energy value of $\sim$75 kJmol^{-1} for the appearance of serrations. This is true for the vacuum-annealed, partially denitrided and irradiated mild steels.

From earlier discussion, it has been observed that the appearance and disappearance of serrations depend on nitrogen concentration. This is expected since the ending of the serrations also correlates with Cottrell or Snoek drag with an inverse concentration dependence of the strain rate. However, Keh et al. [29] and Roberts and Owens [30] found that

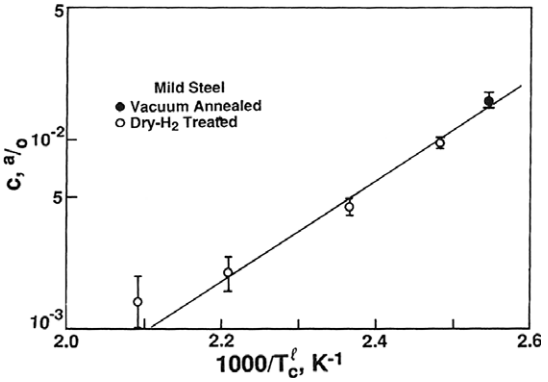

Fig. 13. The variation of concentration of nitrogen as a function of lower critical temperature.

the disappearance of serrations is concentration-independent that might be due to quenching of samples from high temperature [24]. The lower yield stress is independent of the temperature and strain rate (i.e. athermal) at the onset of unstable plastic flow, but it changes with increasing interstitial content as depicted in Fig. 14. The critical stress for the appearance of serrations is given by the following equation:

$$\sigma_c = 85.98 + 3.596 \times 10^5 c, \tag{5}$$

where c is the atomic fraction of nitrogen.

Using the models based on solute drag as described by Cottrell and Snoek, Roberts and Owens [30] derived the relation:

$$\frac{d\tau_s^*}{dc} = \frac{KA}{ba^3}, \tag{6}$$

where K is a constant, b the Burgers vector, a the lattice parameter, and A the Cottrell drag constant which is in turn related to the effective radius of the atmosphere l by

$$l = \frac{A}{kT}. \tag{7}$$

Consideration of the lower critical temperature at a specific strain rate as a function of the nitrogen concentration provides a means for evaluating the density of mobile dislocations using models based on Cottrell and Snoek drag. According to the Cottrell drag, the pertinent equation is:

$$\rho_m = \frac{\dot{\varepsilon}}{4bDkT_c^l}, \tag{8}$$

while for the Snoek drag, the relevant relation is

$$\rho_m = \frac{\dot{\varepsilon}a^2kT_c^l}{24bAD}. \tag{9}$$

Here ρ_m is the mobile dislocation density, $\dot{\varepsilon}$ is the strain rate, A the force constant, a the lattice parameter, k the Boltzmann's constant, T_c^l is the lower critical temperature (for the appearance of serrations), and D the impurity diffusivity at T_c^l.

Fig. 15 depicts the mobile dislocation density evaluated from Cottrell drag model (following Eq. (8)), versus nitrogen concentration in double-logarithmic scale. The dislocation density increases as the nitrogen concentration increases with possible saturation at high values. While the dislocation density calculated from the Cottrell drag model is $\sim 10^7$ cm^{-2}, the Snoek locking leads to a much lower value of dislocation density on the order of 10^4 cm^{-2}. Hence, Snoek locking may not be important in the

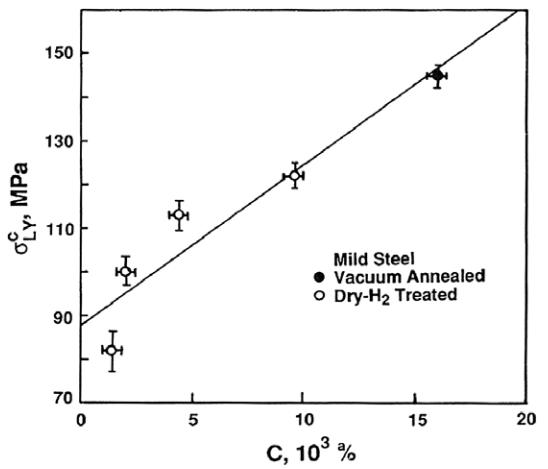

Fig. 14. The lower yield stress for the appearance of serrations as a function of nitrogen concentration.

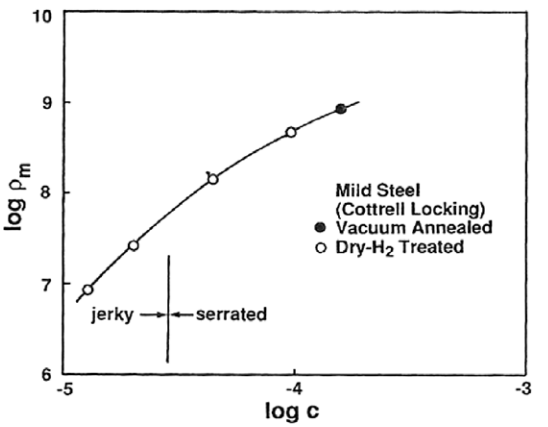

Fig. 15. Mobile dislocation density (in cm^{-2}) versus nitrogen concentration (atom fraction).

case considered here. It is interesting to note that the results from both the serrated flow at higher nitrogen concentrations and jerky flow at very low nitrogen concentrations followed the same curve in Fig. 15. This in turn means that the Cottrell locking is the dominant mechanism for the unstable flow observed here. We also note that the increase in the dislocation density with c is consistent with Fig. 14. It is important to note that the foregoing analysis did not consider the neutron radiation effects, but as discussed earlier the situation will be much like the DSA behavior of partially denitrided steel. However, the lack of quantitative information on the concentration of nitrogen in solution following radiation exposure precludes further analyses.

3.2. A516 Grade 70 Steel

Various researchers have shown that DSA can also occur in low alloy steels albeit at a lesser extent [31,32]. Here we consider the A516 Gr.70 steel commonly used for reactor support structures and summarize its fracture behavior. The load–elongation curves of this material (unirradiated) at different test temperatures are shown in Fig. 16(a). There are less prominent serrations in the curves up to a temperature of 473 K, as compared to the ones noted in the mild steel response. These serrations develop due to DSA during tensile straining. On the other hand, following neutron irradiation (a fluence of 2×10^{18} n/cm^2) the serrations mostly disappeared from the curves as shown in Fig. 16(b) up to 673 K.

Fig. 17(a) and (b) depicts the temperature dependence of the yield stress and elongation, respectively, under both unirradiated and irradiated conditions. Usual radiation hardening is observed at temperatures below 473 K. The elongations of the irradiated material at 373 and 473 K are higher than the unirradiated one. In this temperature range, IIAs and radiation-produced defects interact,

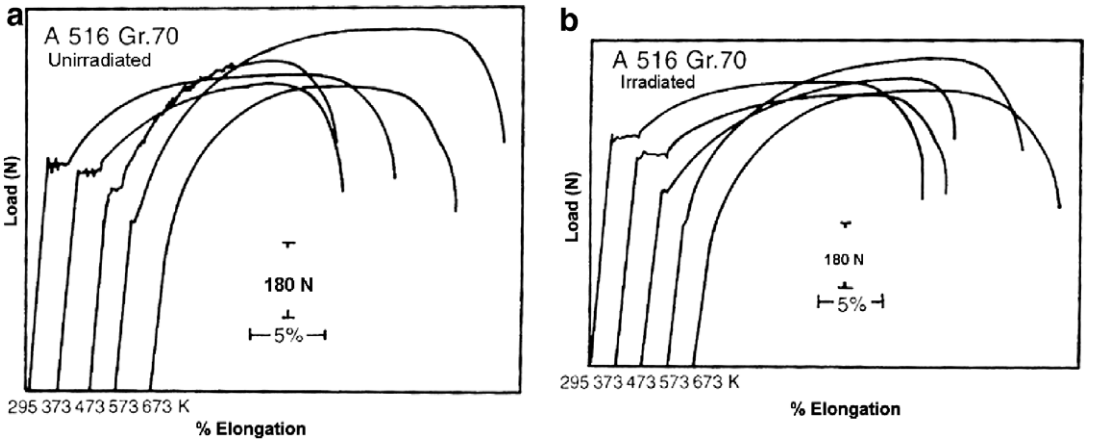

Fig. 16. Load–elongation curves for A516 Gr.70 steels (a) before and (b) after irradiation.

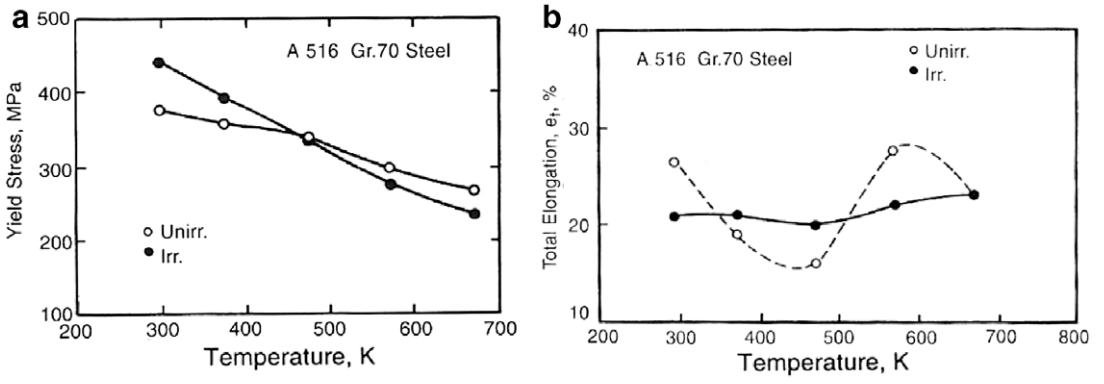

Fig. 17. Temperature dependence of (a) yield stress and (b) total elongation for A516 Gr.70 steel in both unirradiated and irradiated conditions.

and DSA is suppressed as it was witnessed in mild steel. At higher temperatures at 573 K and beyond, reduction in ductility was noted following radiation where DSA is absent in the unirradiated material. At still higher temperatures, the ductility of the irradiated steel becomes essentially equal to that before irradiation due to the annealing of radiation defects.

The DSA effects are more clearly noted in low strain rate three-point bend tests (Fig. 18) when the total energy to fracture is plotted versus test temperature. It should be noted that this temperature regime corresponds to upper shelf region in the Charpy energy; however, distinct dips are noted in the energy at temperatures between 400 and 650 K where serrated yielding is noted. The dip noted here is sensitive to the applied strain rate and at very high strain rates such as in Charpy impact tests, such dips are expected to occur at much higher temperatures than those commonly used. This is the reason why the vast amount of Charpy data on RPV steels does not reveal the effects of DSA [1]. As noted in Fig. 18, radiation exposure resulted in decreased toughness at low and high temperatures beyond the DSA regime while a slight increase is noted in the temperature region where the unirradiated material exhibited DSA and distinct drop.

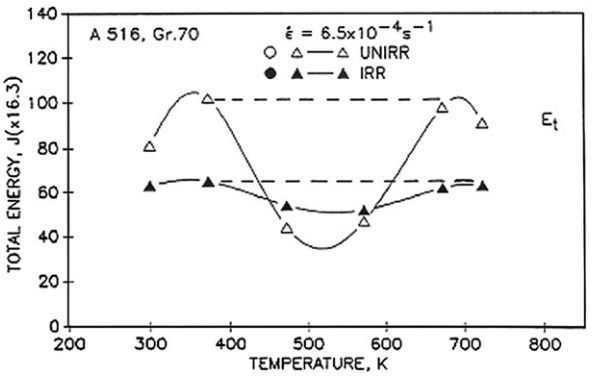

Fig. 18. Fracture energy versus test temperature before and after neutron irradiation.

The stress–strain curves (in Fig. 16) are used to calculate the source and the friction hardening components in unirradiated and irradiated materials. Fig. 19(a) illustrates the variation of friction stresses as a function of test temperature. Here the friction stress components are higher in the irradiated material than the unirradiated below the DSA range ($\leqslant$473 K) due to irradiation induced defects. At higher temperatures not much difference is observed perhaps due to the annealing of radiation-produced defects. Temperature variation of the source hardening is included in Fig. 19(b) which shows decreased values following radiation due to the decreased IIAs in solution. At high temperatures no source hardening is noted due to no locking of the dislocation sources by interstitial atoms at these temperatures. It will be interesting to examine the DSA and irradiation effects on fracture toughness (J_{1C}) through fracture mechanics testing such as single specimen unloading compliance technique [33] that will be of technical significance.

4. Conclusions

In this paper, we reviewed the influence of radiation on mechanical properties (strength, ductility and toughness) for mild steels and a ferritic RPV steel. In mild steel, it is shown that dynamic strain aging and radiation-produced defects can act synergistically culminating in the increase of toughness even when radiation hardening is present. However, this effect is observed in a particular regime of temperatures, strain rates and neutron fluences. A

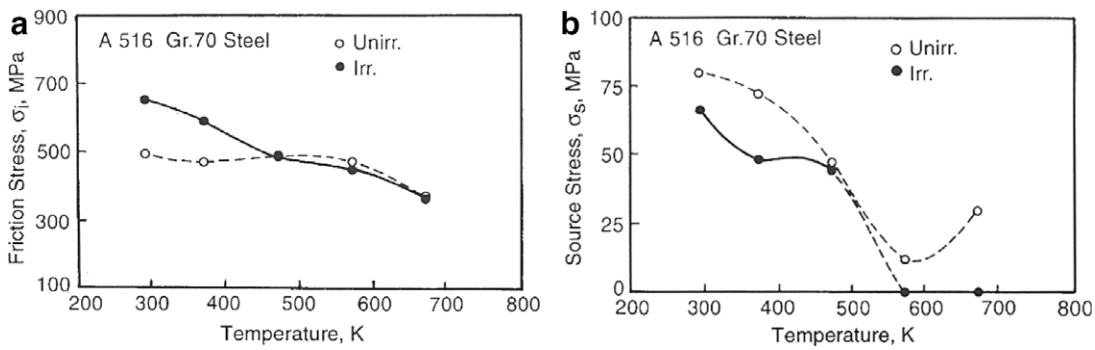

Fig. 19. Temperature variation of friction (a) and source (b) stress components for unirradiated and irradiated A516 steel.

similar effect of radiation is also observed in partially denitrided mild steel, and a plausible physical interpretation of the phenomenon is presented. It is found that interstitial impurity atoms interact with the radiation-produced defects thereby reducing their effective concentration in solution. Thus, dynamic strain aging effects are suppressed following radiation exposure. Radiation hardening effects in mild steel and the RPV steel are elucidated in terms of friction and source hardening contributions. It was substantiated that following neutron radiation exposure the friction hardening component increases whereas the source hardening term decreases. These findings have an important bearing on our ability to predict the change in DBTT following radiation exposure.

References

[1] L.E. Steele, ASTM STP 784 (1983) 227.
[2] K.L. Murty, J. Met. 37 (1985) 34.
[3] G.E. Lucas, G.R. Odette, E. Mader, F. Haggag, R. Nanstad, Proceedings of the Fifth International Symposium on Environmental Degradation of Materials in Nuclear Power Systems – Water Reactors, American Nuclear Society, 1992, p. 696.
[4] M.S. Wechsler, K.L. Murty, Metall. Trans. 20A (1989) 2637.
[5] G.R. Odette, B.D. Wirth, D.J. Bacon, N.M. Ghoniem, MRS Bull. (March) (2001) 176.
[6] E.O. Hall, Yield Point Phenomenon in Metals and Alloys, Macmillan, London, 1970.
[7] L.P. Kubin, Y. Estrin, J. Phys. III 1 (1991) 929.
[8] G.E. Dieter, Mechanical Metallurgy, 2nd Ed., McGraw-Hill, New York, 1976.
[9] K.L. Murty, D.J. Oh, Scripta Metall. 17 (1983) 317.
[10] D.R. Olander, Fundamental aspects of nuclear reactor fuel elements, Energy Research and Development Administration, Document# TID-26711-P1 (1976) 418.
[11] M.A. Adams, J. Sci. Instrum. 36 (1959) 444.
[12] K.L. Murty, J. Nucl. Mater. 270 (1999) 115.
[13] K.L. Murty, Mater. Sci. Eng. 59 (1983) 207.
[14] A.H. Cottrell, Proceedings of the Conference on Brittle Fracture in Metals, in: UKAEA Rep. IG145 (RD/C), May 1959, UK Atomic Energy Authority, 1957.
[15] M. Castagna, A. Ferro, F.S. Ross, J. Sebille, ASTM STP 426 (1967) 3.
[16] L.P. Trudeau, J. Iron Steel Inst. 69 (1961) 382.
[17] R.W. Nichols, D.R. Harries, ASTM STP 341 (1963) 162.
[18] M.J. Makin, F.J. Minter, Acta Metall. 8 (1960) 691.
[19] E.O. Hall, J. Iron Steel Inst. 10 (1952) 331.
[20] M.S. Wechsler, Trans. ASME 101 (1979) 114.
[21] J.G.Y. Chow, S.B. McRikkard, D.H. Gurinsky, ASTM STP 341 (1963) 46.
[22] E.A. Little, D.R. Harries, Met. Sci. J. 4 (1970) 195.
[23] K.L. Murty, E.O. Hall, ASTM STP 611 (1976) 53.
[24] K.L. Murty, S.T. Mahmood, ASTM STP 1046 (1983) 422.
[25] J.E. McLennan, E.O. Hall, J. Aust. Inst. Met. 8 (1963) 191.
[26] H. Wagenblast, A.C. Damask, J. Phys. Chem. Solids 23 (1962) 221.
[27] K.L. Murty, Nature 308 (1984) 51.
[28] A. Van de Beukel, U.F. Kocks, Acta Metall. 30 (1982) 1027.
[29] A.S. Keh, Y. Nakada, W.C. Leslie, in: A.R. Rosenfield, G.T. Hahn (Eds.), Dislocation Dynamics, McGraw-Hill, New York, 1968, p. 381.
[30] M.J. Roberts, W.S. Owens, Metall. Trans. 1 (1970) 3203.
[31] Y.H. Jung, K.L. Murty, ASTM STP 956 (1987) 395.
[32] J.H. Hong, K.L. Murty, in: Proceedings of ASM Symposium on 'Microstructure and Mechanical Properties of Aging Materials', American Society for Metals, 1992, p. 391.
[33] C.S. Seok, K.L. Murty, Int. J. Pres. Ves. Pip. 76 (1999) 945.